Forces and flow structures evolution on a car body in a sudden crosswind

Raffaele Volpe [a,*], Valérie Ferrand [b], Arthur Da Silva [a], Luis Le Moyne [a]

[a] Laboratoire DRIVE, Institut Supérieur de l'Automobile et des Transports, Université de Bourgogne, 49 rue Mademoiselle Bourgeois, 58000 Nevers, France
[b] Université de Toulouse, Institut Supérieur de l'Aéronautique et de l'Espace (ISAE), 10 avenue Edouard Belin, 31400 Toulouse, France

Keywords:
Unsteady aerodynamics
Unsteady crosswind
Unsteady efforts
PIV
Vortices
Road vehicles

A B S T R A C T

A vehicle driver is commonly exposed to strong side air flows, for example when passing through a wind gust. The aerodynamic efforts generated in these situations may induce undesired lateral deviations, which can lead to dramatic effects, if the driver is surprised. In order to simulate a sudden yaw angle change on a moving vehicle, a double wind tunnel facility, adapted from the one of Ryan, Dominy, 2000. Wake Surveys Behind a Passenger Car Subjected to a Transient Cross-wind Gust. SAE Technical Paper No. 2000-01-0874 is developed. Two Windsor car body models, differing from their rear geometry, are analysed. The transient evolution of the side force and yaw moment aerodynamic coefficients are interpreted in connection with the unsteady development of the flow, based on TR-PIV and stereoscopic PIV measurements. Our analysis shows that the region which is most sensitive to crosswind is located at the rear part of the leeward flank. However, changes in the rear geometry (from squareback to fastback body) only affect the established lateral coefficients values while transient duration and the force overshoots appear not to be significantly modified. Furthermore, the circulation of the most energetic leeward vortex appears to be correlated with the lateral coefficients transient evolutions.

1. Introduction

It is a relatively common experience, when travelling by car, to come across any kind of unsteady side wind, for example a natural wind gust or simply the air mass displaced by the vehicle arriving from the opposite direction. It is also known that great care has to be taken when driving during these short lapses of time, because the pressure imbalance between the windward and the leeward flank generates unsteady aerodynamic forces. These efforts are a potential source of hazard, since the vehicle can be deviated from its trajectory by the combined action of side force and yaw moment. More likely in the case of buses, trucks or lightweight trains, the vehicle can be also overturned by the effect of roll moment, as it has been detailed by Baker (1986). As a matter of fact, in the quasi-steady analysis held by Hémon and Noger (2004), it was demonstrated that when a vehicle is subjected to a steep change of wind direction, transient growth of energy occurs, this causing dynamic instability. Moreover, the driver himself can negatively affect the vehicle stability, if he is surprised and accidentally over-corrects the steering angle, (Emmelmann, 1998). The dynamic stability of a given vehicle to a wind gust can be estimated starting from non-linear vehicle models. However, in order to close these models and calculate vehicle trajectory, it is necessary to give as an input the aerodynamic forces evolutions, as recommended by Gilliéron and Kourta (2011).

For many years, it has been thought that lateral forces evolutions could be considered as quasi-static, and that it would be sufficient to measure the steady force coefficient of a static yawed model to predict vehicle behaviour in crosswind. However, Beauvais (1967) showed that the unsteady yaw moment peak can be 40% greater than the corresponding steady effort, if the yaw angle is higher than 10°. This means that it is necessary either to model unsteady effects from the steady measurements, or to reproduce directly a wind gust by means of adapted test benches. In next paragraph, a brief summary of experimental and numerical techniques, used for estimating the unsteady lateral forces evolution is presented.

1.1. Experimental and numerical simulation of lateral wind gusts on ground vehicles

The most realistic approach to experimentally simulate a wind gust on ground vehicles is to propel a vehicle model on a rail trough the flow generated by a lateral wind tunnel. When performing these tests, the main goal is usually to evaluate the ratio between the unsteady efforts peaks and the corresponding

* Corresponding author: Tel.: +33 5 61 33 81 47; mob.: +33 6 83 49 05 38.
E-mail address: raffaele.volpe@u-bourgogne.fr (R. Volpe).

values resulting from the steady state case. Most of the authors, such as Beauvais (1967), Cairns (1994), Baker and Humphreys (1996), Chadwick (1999) agree that this ratio is 1.2 to 1.5, whereas Stewart (1977) and Kobayashi and Yamada (1988) measured yaw moment peaks up to more than the double of the static force. Also, Baker and Humphreys (1996) studied the influence of the yaw angle and found out that the peak overshoot tends to disappear in the range between 40° and 60°. Another result of interest is the establishment time of the force coefficient, expressed as the number of times the vehicle has travelled its own length through the side wind wall. Little agreement was found between the authors: Beauvais indicates the establishment time after 4 vehicle lengths, but in Cairns and Chadwick tests, where a 5 vehicle wide gust was employed, no force establishment was seen. In Stewart's case, this time is dependent on the vehicle geometry. Such scattered data between the different authors can derive from the main drawbacks of this kind of test bench, that is the presence of noise in the signal and the difficulty in having data with high repeatability. The noise mainly derives from both the vibrations induced by the small irregularities on the rail and the resonance frequencies of the moving facility itself, excited by the wind tunnel flow. An elevated number of test repetitions is then needed and great care has to be taken during the processing data phase.

This is one of the reasons why the steady wind tunnel tests with yawed vehicle have not been completely disregarded. As a matter of fact, when the side wind is stochastically expressed by its spectrum, it is possible to obtain the corresponding spectra of the unsteady force coefficients, by means of a correction function called "aerodynamic admittance", which also requires the steady coefficients values. This function is defined in the complex domain and has been described by Cooper (1984) and Baker (1991a). This aerodynamic admittance can be measured from static yawed model tests, at high turbulence intensity, or by means of the test bench proposed by Bearman and Mullarkey (1994), in which a static model is subjected to a sinusoidal flow created by an upstream series of oscillating profiles. The latter tests have to be repeated at different oscillation frequencies, to collect the information for the whole spectrum. Furthermore, the aerodynamic admittance can be approximated with the formulae proposed by Baker (2010) or estimated with the model of Tomasini and Cheli (2013). Once the aerodynamic admittance is known, it is possible to derive a weighting function which relates the force evolution to the side wind history with a convolution integral.

Another advantage of static tests is that it is simpler to retrieve information about the flow field, which mainly presents two different patterns, depending on the yaw angle, as described by Baker (1991b) and numerically confirmed by Khier et al. (2000). For small yaw angles, from 0 to 30°, the vehicle can be considered as a slender body, and a detailed description of the flow field can be found in the work of Mair and Stewart (1985). A schematic drawing of this kind of flow is depicted in Fig. 1, for a simplified shape of squareback vehicle. In the slender body flow, the most energetic structure, Γ_A, originates from the front of the vehicle, near the roof, and expands along the leeward flank. A second twin vortex Γ_B originates from the vehicle underbody. A last vortex, Γ_C, develops from the windward side of the roof. The intensity and the size of these structures grow up with the yaw angle, in the range of 0°–30°.

Chiu and Squire (1992) expanded this study to higher yaw angles. In particular, they showed that for very high yaw angles, starting from 60°, vortex shedding is visible in the wake, since the vehicle can be considered as a bluff body. In the intermediate range between 30 and 60°, they also showed that the vortex shedding wake and the flow pattern from Fig. 1 coexist. More precisely, there is a dynamical switch between the two flow configurations.

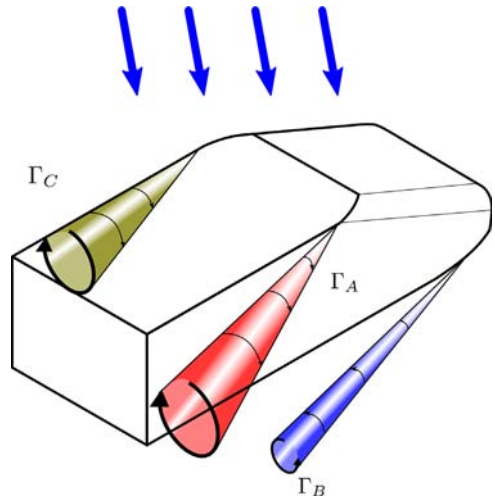

Fig. 1. Vortices representation for a vehicle subjected to steady crosswind, $0° < \beta < 30°$. Image inspired by Baker (1991b).

Other kinds of side wind test benches have been conceived, in order to join the advantages of both previous approaches. For example, Garry and Cooper (1986) mounted their 1—box vehicle models on an oscillating turntable, situated in a middle of a wind tunnel. A similar technique was used by Cairns (1994), except that a sudden yaw angle change was imposed, with no oscillation. No force overshoot was seen. However, in both cases, the unsteady effort appeared to be delayed, if compared to the steady effort at the equivalent yaw angle. The work of Chometon et al. (2005), based on PIV measurements, allowed to give an explanation. In fact, the formation of flow field vortices is not instantaneous, but occurs with a phase shift. In particular, Ferrand and Grochal (2012) proved that the phase shift of the side force is greater in the rear part of the body.

Another interesting kind of test bench is the moving side jet facility proposed by Dominy (1991). With this approach, the moving model principle is completely reversed: the model is now static, and two wind tunnels produce an unsteady side wind. The main wind tunnel is classically used to simulate the streamwise vehicle motion, while the auxiliary one produces the wind gust. The passage of the auxiliary air flow in the measurement region is driven via a user-controlled intercommunication system. In the main results presented in Ryan (2000), Ryan and Dominy (2000), side force and yaw moment overshoots were seen at the gust entrance, varying from 7% to 55%, depending on the studied geometry. The flow establishes after 7 vehicle lengths. The flow field was also inspected by hot-wire probing and the origin of force overshoots was attributed to the delayed formation of the separation region near the front leeward corner.

As far as the numerical simulations are concerned, the rigorous reproduction of a vehicle moving through a wind wall is not an easy task. As a matter of fact, sliding or deforming meshes are needed, which can lead to convergence difficulties and calculation time enhancement. At first, 2D analyses on simplified car bodies, overtaking each other, were made by Clarke and Filippone (2007) and Corin et al. (2008). In particular, in the latter work, it was found that steady simulations underestimate the unsteady results, as seen in experiments. Recently, a simulation of a heavy-duty truck crossing a wind gust has been made by Nakashima et al. (2012). In this simulation, the fluid equations, in which the large eddy simulation (LES) approach has been used, were coupled with a 3 degree-of-freedom model of the vehicle's dynamic motion. A simple driver model was also added. The calculated yaw moment presents overshoots up to 200% at the entrance and at

the exit of the gust. The difference with other data can derive from the huge lateral area of the vehicle.

The most used approach, when simulating wind gust effects by CFD, is to use a grid either static or moving at a constant speed, with the introduction of a side air flow, by using time-dependent boundary conditions. This principle is somehow similar to the one of Dominy's moving side jet test bench. Favre and Efraimsson (2011) studied the reliability of this technique for crosswind scenarios, for estimating the unsteady drag variation. In particular, it decreases until 40% when entering the gust and becomes 90% higher than in the longitudinal steady simulation when exiting. No side force overshoot was seen. In the simulation of Tsubokura et al. (2010), a realistic vehicle shape was used. Their results confirm the conclusions of Beauvais. They also found that vertical force, roll and yaw moment need longer time to establish. Krajnovic et al. (2012) simulated the passage of a train exposed to a 45° yaw angle gust, obtaining a good agreement with experimental data and a 30% yaw moment overshoot.

1.2. The objective of this work

This state of the art indicates that there are nowadays many data about the temporal evolution of aerodynamic forces applying on road vehicles in crosswind gust situations, even if some discordance exists between authors. However, the unsteady development of flow structures in such situations has been hardly explored yet. In this paper, the evolution of the aerodynamic tensor components that mainly affect vehicle dynamic lateral stability, the side force and the yaw moment, will be analysed in connection with the unsteady flow field. The velocity field will be characterized with particle image velocimetry (PIV) techniques, including stereoscopic and time resolved PIV. As far we know, there is no previous work in which this experimental instrumentation has been used for ground vehicle unsteady crosswind study. We remark that our final goal is not to faithfully reproduce a model scaled wind gust, the interest is rather to understand the aerodynamic response of a given vehicle shape to a sudden wind direction change.

The chosen experimental approach is the moving side jet facility proposed by Dominy (1991), since it avoids any noise source induced by a moving vehicle. Moreover, PIV measurements can be more conveniently performed on a static model. These are the reasons why the ISAE started developing a similar facility in 2007, getting inspiration by the evolution proposed by Dominy and Ryan (1999). The detailed description of the test bench is found in Section 2, its performances and the main characteristics of the resulting unsteady flow field are reported in Section 3. Section 4 introduces at first the results of the unsteady aerodynamic forces and then of the flow field evolution. Finally, an analysis focusing on their mutual correlation is presented.

2. Experimental set-up

2.1. Experimental test bench characteristics

The test bench developed by the ISAE consists in a double wind tunnel, whose communication is controlled by a system of electrically driven shutters, located in 20 channels inside the auxiliary wind tunnel, Fig. 2. The goal of the shutter system is to create a side moving jet, mimicking a moving wind gust.

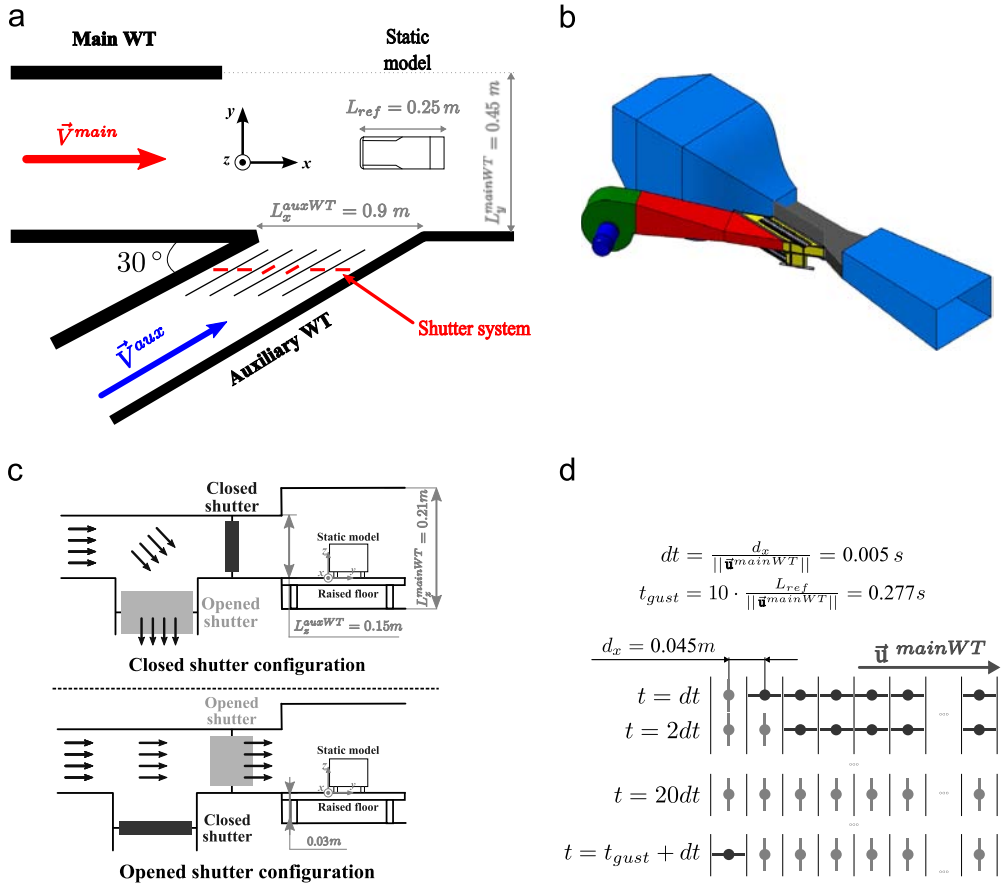

Fig. 2. The "rafale latérale" test bench: functioning diagram, (a), CAD drawing (b), projected side view of a channel of the shutter system, (c), opening/closing shutter sequence, (d).

The facility test section is semi-enclosed, in order to permit the evacuation of the auxiliary wind tunnel air flow. This also prevents any blockage effect. The test section dimensions are $L_y^{mainWT}=0.45$ m, $L_z^{mainWT}=0.21$ m; the final section of the auxiliary wind tunnel is $L_x^{auxWT}=0.9$ m, $L_z^{auxWT}=0.15$ m wide. The relative angle between the wind tunnels is 30°.

The auxiliary wind tunnel actually has two outlets, one of which is connected to the test section. The interior of this wind tunnel is divided in 20 channels, each one presenting a couple of antagonist shutters for flow control. Whenever a shutter of the test section outlet is closed, its antagonist is opened, allowing the evacuation of the auxiliary wind tunnel airflow (Fig. 2c). The shutters configuration is reversed if a sudden change of side wind is simulated. This solution ensures mass flow conservation through every channel whatever the number of the test section outlet shutters is. Every shutter is opened and closed by means of an electromagnet–spring system, remotely controlled by a LabView interface. In order to make the auxiliary air flow move along the main wind tunnel, the test section outlet shutters are not all opened at once, but one by one, in sequence. The time between the opening of one door and the following is set up for having the "front" of the jet moving at the same speed of the main wind tunnel; the opening time of a single shutter corresponds to the imposed wind gust duration. The shutters then close sequentially with the same law (see Fig. 2d).

The main wind tunnel velocity, was set to $\|\vec{V}^{main}\|=9$ m/s, whereas the auxiliary wind tunnel velocity is $\|\vec{V}^{aux}\|=10.39$ m/s. The corresponding Reynolds number is $\mathrm{Re}=1.73\cdot10^5$, calculated with the latter velocity, the model reference length $L_{ref}=0.25$ m, and with the air temperature $T=20$ °C at atmospheric pressure.

2.2. Windsor body

The car-body used for this study is the Windsor model (see Fig. 3). Its length, $L_{ref}=0.25$ m, and its frontal surface, $S_{ref}=0.00644$ m², will be used as references when calculating the aerodynamic force coefficients or any other non-dimensional quantity (expressed, in the following, by means of a "+" exponent). The model was installed over a raised floor, aligned with the floor of the auxiliary wind tunnel (see Fig. 2c). The model is supported by four cylindrical feet, ensuring a 12 mm ground clearance. Two Windsor body configurations were studied, a squareback geometry and a one presenting a 25° rear window slant (referred, in the following, as "fastback" configuration). As shown by Howell (1993), when subjected to steady longitudinal flow, the drag of a Windsor body has the same qualitative behaviour described by Ahmed et al. (1984) for their model. This is because of the different wake topology behind the vehicle rear. If the rear slant angle is between 15° and 30°, a pair of counter-rotating trailing vortices develops from the rear window sides, as drawn in Fig. 4a. Under this slant angle, the near wake is

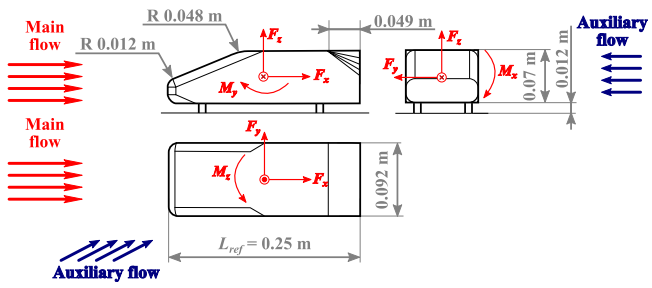

Fig. 3. Windsor body geometry.

dominated by two horseshoe structures, as schematized in Fig. 4b. The Γ_1 streamwise vortices and their coupling with the slant separated region are known to be responsive to the drag crisis observed at the 15° critical slant angle, Hucho (1989). We propose in this paper to identify their contribution to the unsteady response of the aerodynamic tensor in unsteady yaw angle situations.

2.3. Experimental instrumentation

2.3.1. Five component unsteady balance

The aerodynamic forces were measured with a strain gauge balance, embedded inside the Windsor body. The nominal capacity of this instrument is 10 N for the forces and 0.5 N m for the moments. Even if five out of the six force components were measured, we will focus, in this paper, on the most relevant efforts concerning vehicle cross-wind stability, i.e. the side force C_{Fy} and the yaw moment C_{Mz}. The balance was calibrated with a dynamic system composed of a magnetic field generator, inducing a displacement on a coil linked to the exterior shell of the car model. The frequency response function of the instrumented model was obtained. In the unsteady tests, the signal was low-pass filtered at 35 Hz and corrected with the frequency response function. Balance accuracy has been estimated to be 1% for side force and 0.06% for yaw moment.

2.3.2. PIV measurements

Two planes were chosen for the unsteady flow analysis: a horizontal plane passing through the Winsdor body, aiming at exploring flow differences between the front and the rear of the model, and a vertical one behind the vehicle, for the study of the lateral structures development (Fig. 5). A TR-PIV system from Dantec was employed for the horizontal plane. A Nd-YLF laser, with a lengthwave of 527 nm, energy 20 mJ per pulse and a maximal frequency of 10 kHz generated the sheet from the leeward side of the wind tunnel. Transparent Windsor models were specifically created to visualize simultaneously the flow on both lateral sides of the vehicle. The camera was a Phantom v12, with double frame CCD sensor resolution of 1200×800 pixel and maximum sampling frequency of 1 kHz. The sampling frequency of the presented results was set to 500 Hz. The velocity fields were deducted from adaptive cross-correlation of images. A 32 pixel final size of the interrogation area and a 50% overlap granted a spatial resolution of 3.5 mm. Measurements were made in 3 planes, each sizing 127×202.5 mm, centred on the longitudinal axis of the transparent model. The overall TR-PIV plane dimensions are 345 mm by width and 202.5 mm by height. This plane intersects the model at $z^+=0.16$. Concerning the vertical plane, a low frequency stereoscopic PIV system, still from Dantec, was used. The laser was a 532 nm lengthwave Nd-YAG, energy 32 mJ per pulse and maximum frequency of 8 Hz. The cameras were two HiSense Type 11, with a maximal sampling frequency of 4 Hz and CCD sensor resolution of 1280×1024 pixel. The camera sampling frequency was too low for permitting a satisfactory temporal resolution of the wind gust (each test repetition lasting 0.4 s). The PIV system was then synchronised to the test bench controller so that measurements could be started with an imposed time delay. By repeating the measurements for different delays, we have been able to obtain the unsteady flow field at the most interesting moments. Again, the adaptive cross-correlation algorithm was used for the velocity field calculation. The final size of the interrogation area was 32 pixels, with 50% overlap giving a spatial resolution of 2 mm. The measurement plane dimensions are $L_y=167.5$ mm and $L_z=110$ mm, and it is placed 5 mm behind the model back, $x^+=4.36$.

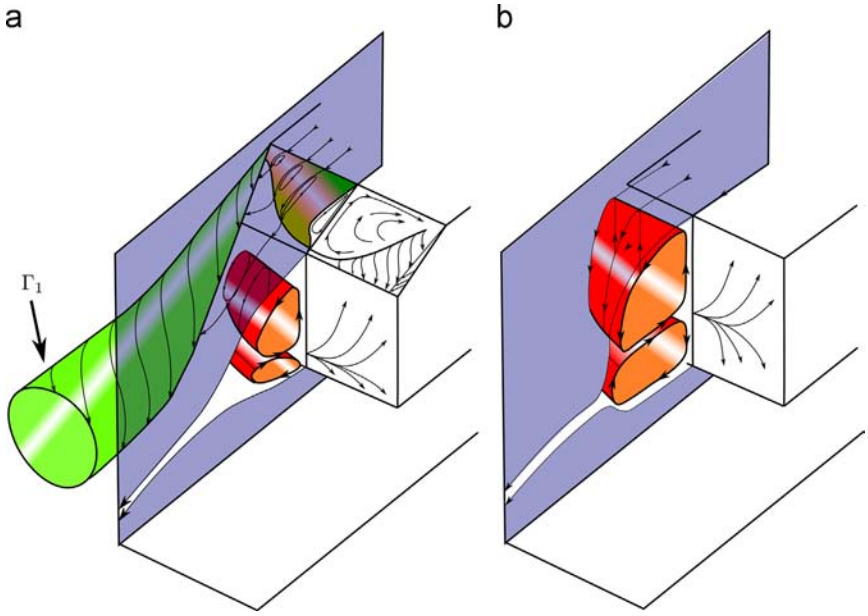

Fig. 4. Flow field on the wake of a simplified vehicle subjected to steady longitudinal flow: fastback case, (a), squareback case, (b). Drawings inspired from Ahmed et al. (1984).

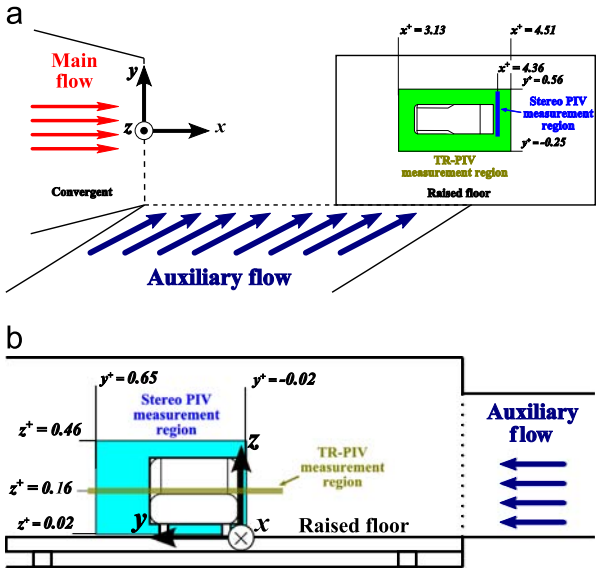

Fig. 5. Locations of the PIV measurements planes. Top view, (a), side view, (b). All coordinates are dimensionless using the model length L_{ref}.

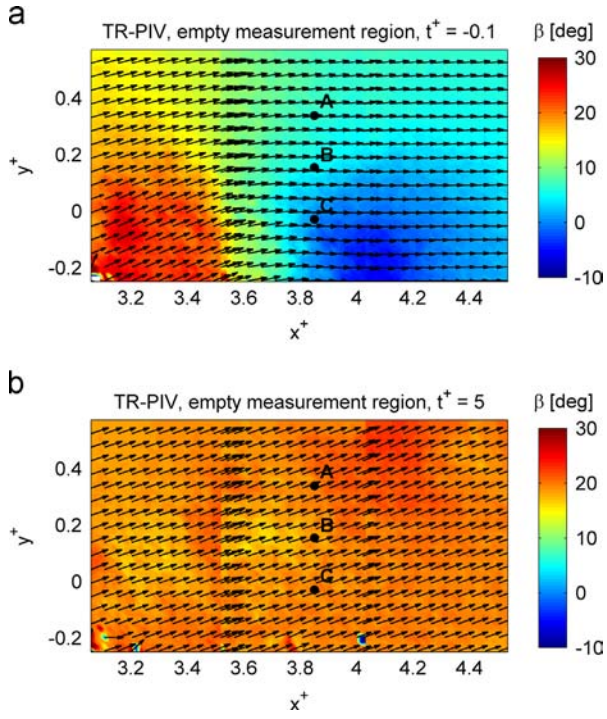

Fig. 6. Empty test bench characterisation, TR-PIV measurements of the unsteady yaw angle field, $t^+ = -0.5$, (a), $t^+ = 5$, (b), $t^+ = 9.5$, (c).

3. Characterization of the generated lateral wind gust

We recall that in the double wind tunnel approach, in order to respect the similitude with the reality, the longitudinal component of the main wind tunnel represents the vehicle speed, whereas the auxiliary wind tunnel velocity is supposed to be the one of the wind, as seen by a driver on board. So the two steady wind tunnel mass flows are set so that the following relations are respected:

$$\|\vec{V}^{aux}\| = \frac{\|\vec{V}^{main}\|}{\cos\ 30^\circ}$$

$$u\rightarrow^{aux} = \vec{V}^{main}, \quad \text{with} \quad \vec{u}^{aux} = \vec{V}^{aux} \times \vec{x}$$

where $\vec{V}^{main}$ and $\vec{V}^{aux}$ are the upstream velocity vectors of the main and the auxiliary wind tunnels, respectively. In our case, $\|\vec{V}^{main}\| = 9$ m/s and $\|\vec{V}^{aux}\| = 10.39$ m/s.

The reference length used in the following is the Windsor body length (L_{ref}=0.25 m, see Fig. 3), whereas the reference velocity is the one of the auxiliary wind tunnel $\vec{V}^{aux}$. However, the reference velocity to normalize the time is the main wind

tunnel velocity $\overrightarrow{V}^{main}$. This choice permits to express time as the number of reference lengths covered by the vehicle in the main flow, so that results can be compared to literature:

$$t^+ = t\frac{\|\overrightarrow{V}^{main}\|}{L_{ref}} \tag{2}$$

Some excerpts from TR-PIV measurements of the empty measurement region are presented in Fig. 6, illustrating the propagation of the side wind, for a simulated crosswind duration $t^+_{gust} = 10$. The results are phase averaged over 15 runs. The represented field is the yaw angle, β, defined as the angle between the longitudinal velocity component, u^+, and the corresponding transverse component, v^+:

$$\beta(t^+) = \arctan\left(\frac{v^+(t^+)}{u^+(t^+)}\right) \tag{3}$$

Temporal origin was shifted so that $t^+ = 0$ corresponds to the instant when the lateral flow head reaches the position of the future model nose.

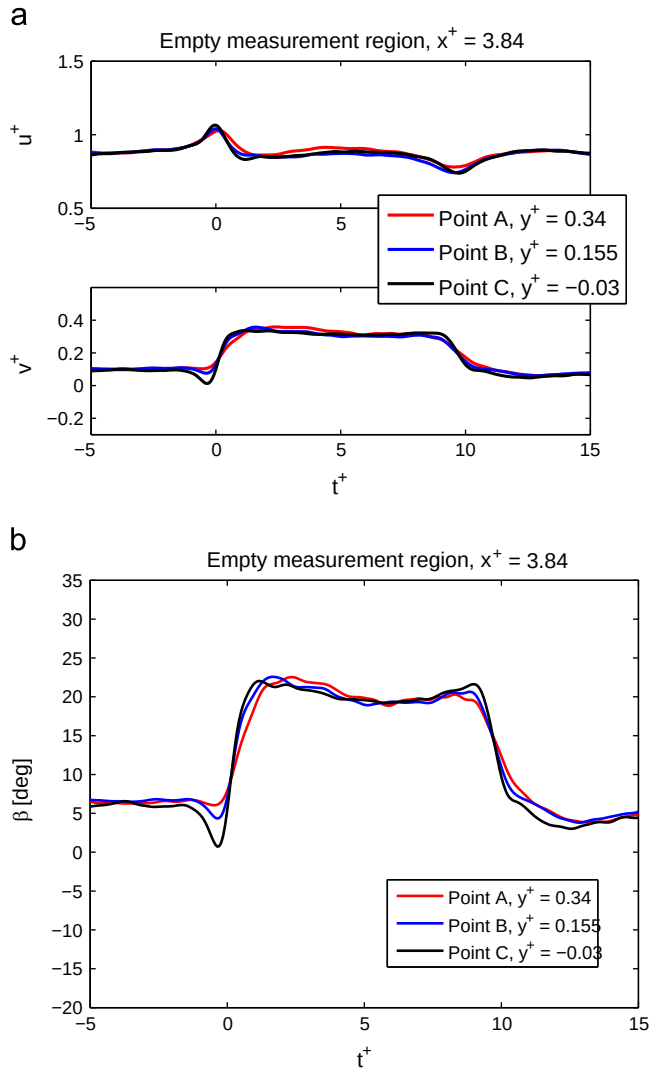

Fig. 7. Empty test bench characterisation, TR-PIV measurements of unsteady velocity components evolution (a) and yaw angle evolution (b) at different distances from the auxiliary wind tunnel exit.

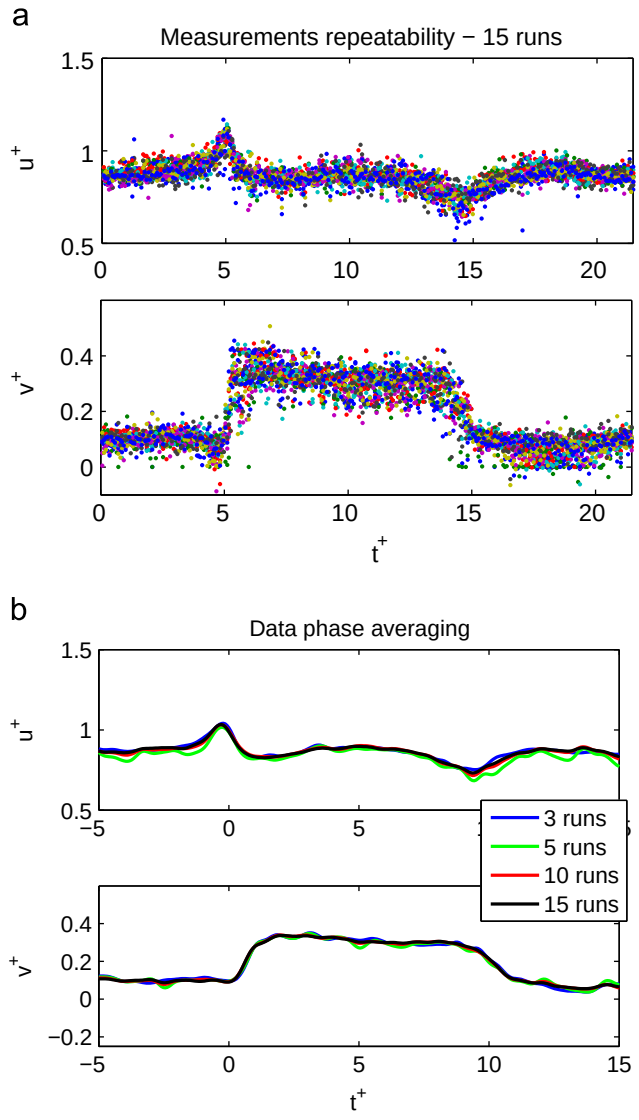

Fig. 8. Test bench repeatability, TR-PIV of unsteady velocity components evolution at position of model mass center: superposition of 15 consecutive runs (a), data phase averaging, (b).

When the auxiliary flow is established, Fig. 6b, the yaw angle is 21°. This value is lower than the 30° angle between the wind tunnels. This is because the auxiliary flow is straightened up by the main wind tunnel. In Fig. 7a and b is presented the evolution of the non-dimensional unsteady velocity components u^+ and v^+ and the one of the resulting yaw angle for the three points marked in Fig. 6. Points A and C are located at mid-length of the model flanks, whereas point B is situated at the future position of the Windsor model mass center. Fig. 8b and Fig. 9a and b also show no spatial gradient in the presented fields, neither when the side wind is established or during the transient propagation of the auxiliary mass flow. The u^+ over and undershoots at $t^+ = 0$ and $t^+ = 10$ are attributed to the transient penetration of head and tail of the secondary flow, as discussed in Volpe et al. (2013).

In the following, our study will focus only on side force and yaw moment, and our dissertation will be regarding especially the flow evolution for $1 < t^+ < 9$, that is when the longitudinal nondimensional velocity has returned to unity and the model is totally dipped in the yawed lateral wind.

In Fig. 8a, the repeatability of the simulated unsteady cross-winds is checked. TR-PIV measurements at the future mass center model position (point B in Fig. 6) of the 15 consecutive runs are

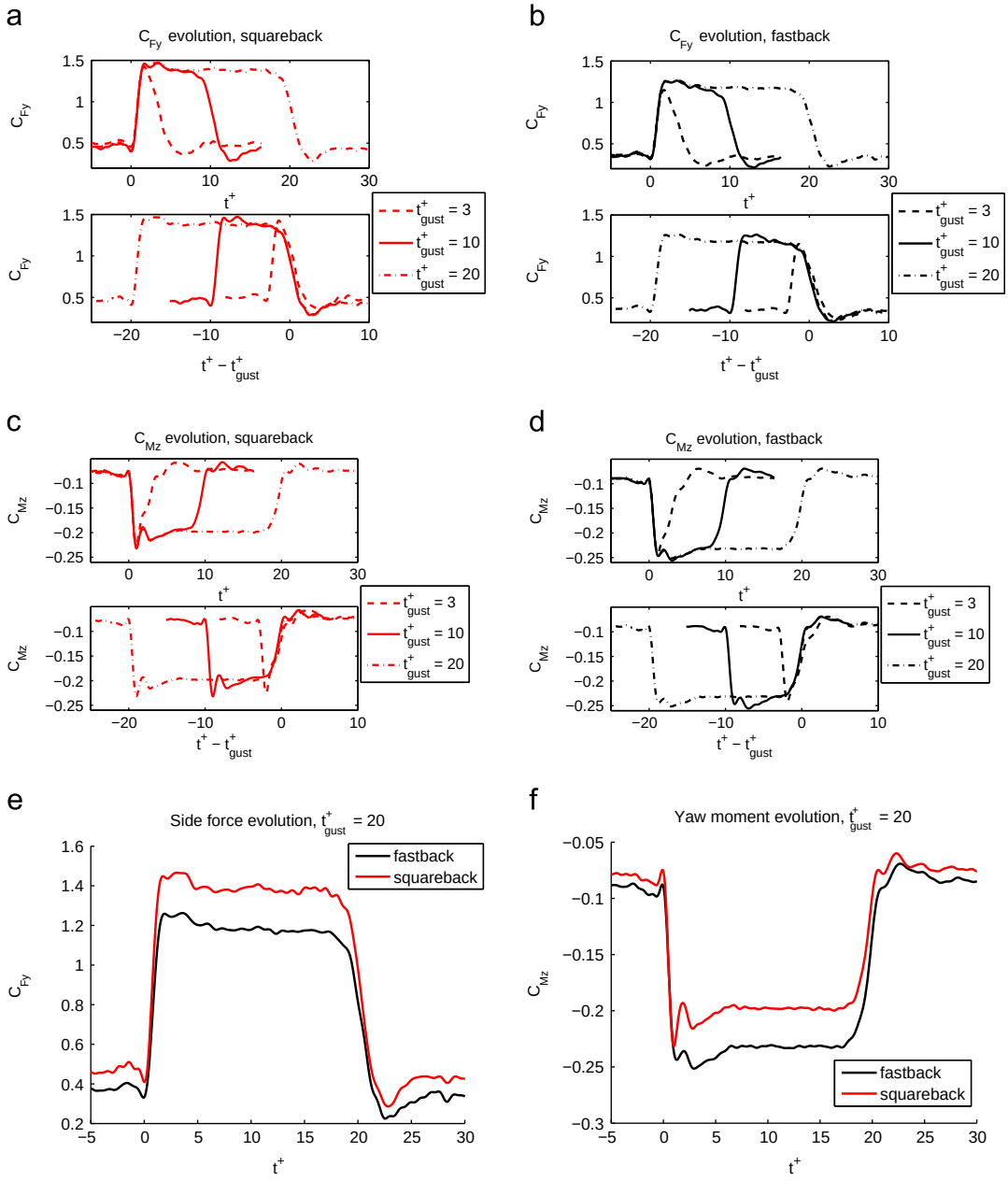

Fig. 9. Unsteady crosswind, experimental aerodynamic lateral coefficients: side force coefficient for the squareback (a) and fastback Windsor models (b); yaw moment coefficient for the squareback (c) and fastback Windsor models (d); model geometry comparison for $t^+_{gust}=20$: side force coefficient, (e), yaw moment coefficient, (f).

superposed. The test bench repeatability is good, the velocity standard deviation being 0.8% of the main wind tunnel velocity. The sensibility of data phase averaging to the number of runs is studied in Fig. 8b. An average over 10 runs is enough to have proper velocities evolutions. However, it was chosen to average the data over at least 15 runs. When presenting the different results, the exact number of repetitions used for averaging will be reported.

4. Car body unsteady efforts and flow field results

4.1. Unsteady efforts on the Windsor body

The temporal evolutions of the lateral efforts, measured by the unsteady balance, are shown in Fig. 9a–d. The presented results are phase averaged over 50 runs. Three different side wind durations were analysed: the same curves are firstly presented as synchronised on the side wind arrival, then time shifted in order to compare their descending fronts. It can be noted that the crosswind duration has no influence in the lateral coefficients evolution, this confirming the high repeatability of the test bench. The coefficients establish, for both model geometries, when $t^+=7$. This result was already seen by Ryan (2000) on the same kind of test bench. Also, it is coherent with the results of Cairns (1994) and Chadwick (1999) obtained from a moving model facility. In their conclusions, they stated that a non-dimensional gust duration of 5 was not enough to let the lateral coefficients establish.

To ease the comparison between the two geometries, the coefficients evolutions are redrawn in Fig. 9e and f, for the longest crosswind duration case. In the presented results, coefficient overshoots are visible after the side wind arrival. In particular,

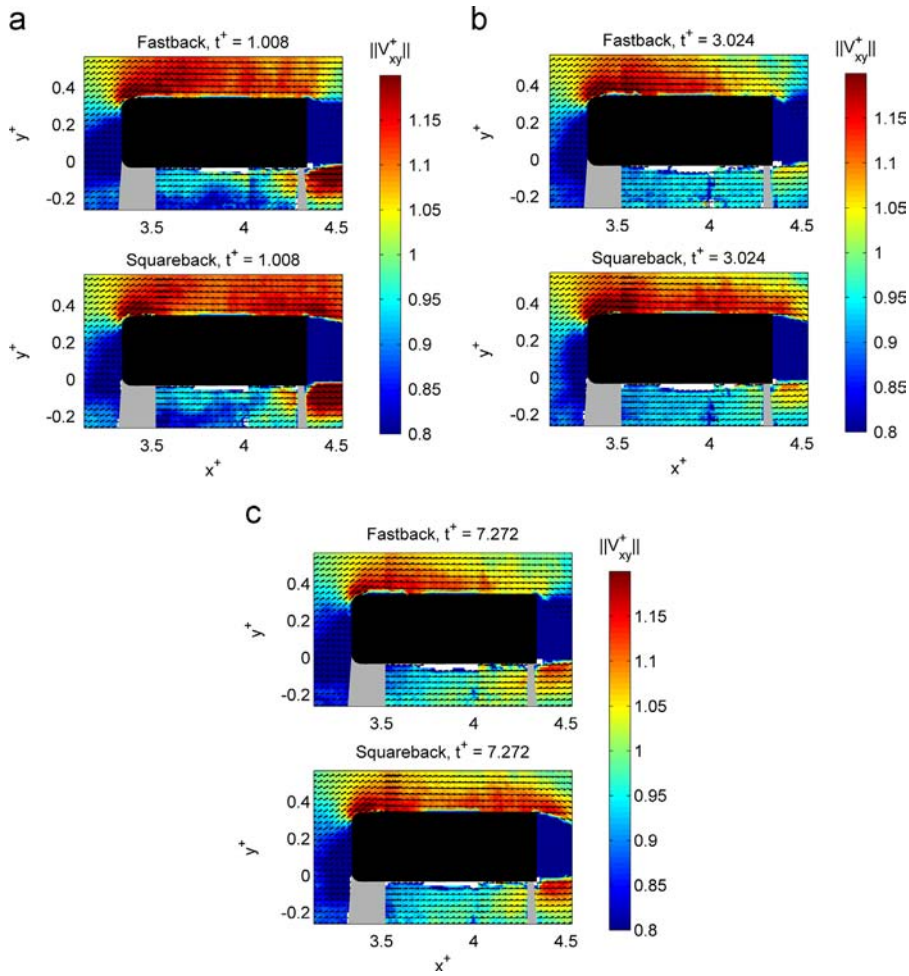

Fig. 10. Unsteady crosswind, TR-PIV measurements of the non-dimensional velocity flow field: $t^+=1.008$, (a), $t^+=3.024$, (b), $t^+=7.272$, (c).

the side force behaviour reaches its maximum at $t^+=1.7$, for both geometries. This maximum is maintained until $t^+=3.4$, then the side force establishes. The side force maximum is greater than its established value by 7%, for both geometries. Let us remark that the lateral efforts maxima are not reached when the car body is entirely dipped in the wind gust ($t^+=1$), but later. This has to be related with the phase delay of the flow field observed in the turntable test benches of Cairns (1994) and Chometon et al. (2005). The temporal behaviour of the side force seems to not be affected by the model rear configuration (i.e. the difference of the two side force coefficients remains constant).

The yaw moment coefficient evolution shows two overshoots, at $t^+=1$ and $t^+=3$, before establishing. The transient behaviour is now dependent upon the geometry. For the squareback case, the peak is reached shortly after the model is fully entered in the side wind ($t^+=1$), while for the fastback, the yaw moment maximum intensity is reached at the second overshoot, $t^+=3$. The TR-PIV measurements (Fig. 12b and c) will show that during this lapse of time the flow is differently organised near the leeward flank of the two geometries, starting from mid-length of the vehicle to the rear. Such different behaviours in the yaw moment have also been observed in the numerical simulations of Favre and Efraissom (2011) on the same model. The peak values exceed by 16% and 10% the established yaw moments, for the squareback and the fastback geometry, respectively. It is worth noting that, starting from the local minimum at $t^+=2$, the difference between the yaw moment coefficients of the two geometries remains constant, as for the side force. This indicates that a change in rear geometry affects the transient behaviour of aerodynamic force or moment in the very first instants after the vehicle has entered the wind gust, then only acts on the established value.

4.2. *Flow field and structures transient response*

In Fig. 10, the TR-PIV velocity field, $V^+_{xy}(x^+, y^+, z^+=0.16, t^+)$, is compared for the two car bodies. Since flow establishment has been seen at $t^+=7$, it was decided to study a crosswind duration of $t^+_{gust}=10$. The presented results are averaged over 15 runs. Three specific instants have been chosen: when the two yaw moment peaks are attained ($t^+=1$ and $t^+=3$) and just after the global lateral coefficients establishment ($t^+=7$). It is remembered that, during these instants, the car body is fully dipped into the auxiliary wind tunnel flow: any difference between the presented fields can be interpreted as representative of the transient response of the flow to a sudden increase of the yaw angle.

In the chosen plane, the most evident flow unsteadinesses are located in the leeward side of the vehicle. Moreover, the velocity field in the rear part of the body presents strong sensitivity to the model geometry. To get a deeper insight, velocity distributions over a horizontal line are plotted in Fig. 11, for different instants. The chosen line is situated 12.5 mm far from the leeward flank. The model extremities correspond to the two vertical dotted lines. Furthermore, the Fig. 12 presents the velocity temporal evolution at 5 points contouring the model, the dotted lines representing the chosen instants from Fig. 11.

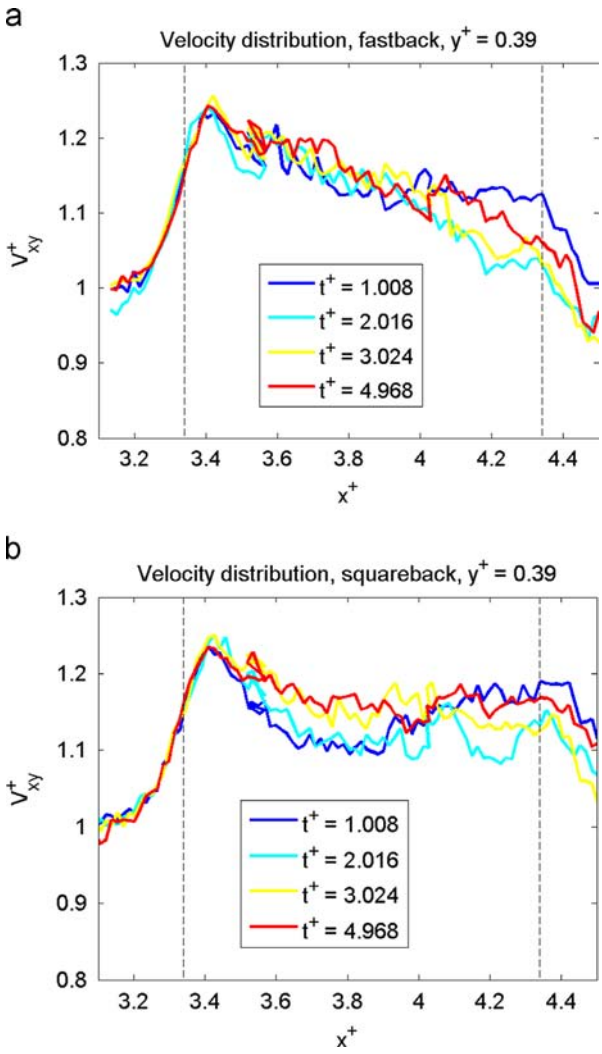

Fig. 11. Unsteady crosswind, TR-PIV measurements of the non-dimensional velocity flow field, velocity distribution at $y^+=0.39$: fastback model, (a), squareback model, (b).

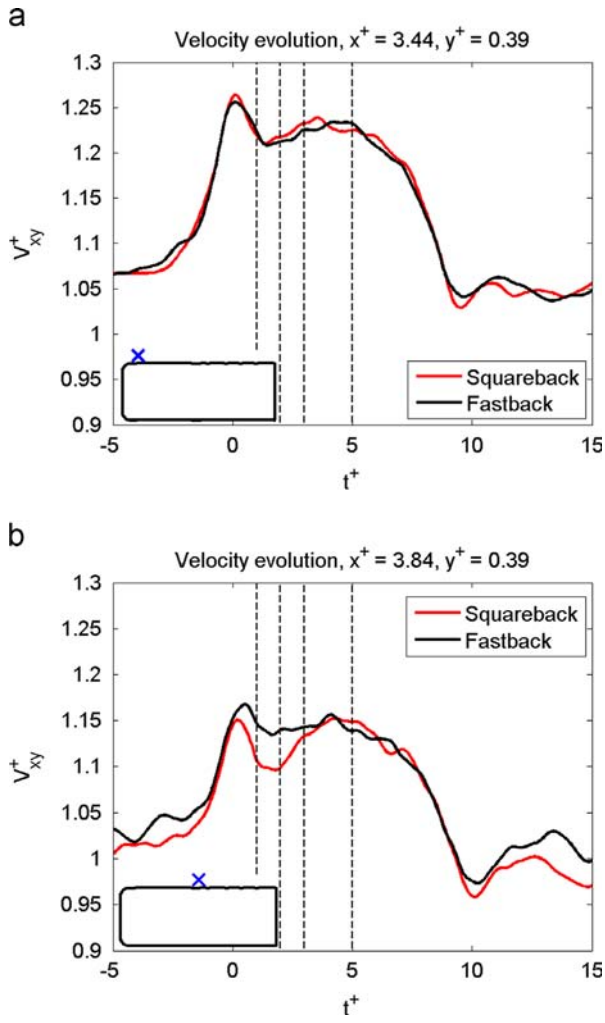

Fig. 12. Unsteady crosswind, TR-PIV measurements of the non-dimensional velocity flow field, velocity distribution at $z^+=0.16$: leeward side, $x^+=3.44$, (a), $x^+=3.84$, (b), $x^+=4.26$, (c), windward side, $x^+=3.86$, (d), $x^+=4.26$, (e).

The higher velocity region at the front of the leeward side ($3.34 < x^+ < 3.56$) is quite stable over time during the transitory period ($1 < t^+ < 5$). On the contrary, the flow does not show an effective establishment at the rear of the leeward flank ($4 < x^+ < 4.34$) during the same period, this confirming the results of Ferrand and Grochal (2012), showing a longer establishment time at the rear of the vehicle. In the accessible region of the windward side, the flow behaves as in the empty test bench case, Fig. 8c, showing overshoots when the head and tail of the lateral wind are passing; no other relevant unsteadiness is visible. The model geometry has little influence on the flow unsteadiness, except for $1 < t^+ < 2$, when a different behavior is visible for $x^+ > 3.8$. As shown in Fig. 12b, the flow around the fastback geometry immediately establishes after the arrival of the side flow head, whereas in the squareback case the flow is stable after $t^+ = 3$; this can be related to the different yaw moment behaviour observed on Fig. 9 during this lapse of time. After $t^+ = 3$, the model geometry affects more the average local value of the velocity in the leeward rear side than the flow temporal response. As shown in Fig. 12, the difference between the two curves tends to remain constant. This absence of unsteady effect is consistent with the temporal evolutions of side force and yaw moment coefficients, observed on Fig. 9e and f.

Since the most relevant differences between the two chosen geometries have been found in the rear leeward region of the vehicle, stereoscopic PIV measurements have been performed in a vertical plane located just downstream the vehicle, Fig. 13a, to identify influential aerodynamic structures at the rear of the body. This time, the opaque Windsor models were used and the unsteady fields were averaged over 20 runs. The vorticity field ω_{yz}^+ is extracted, with:

$$\omega_{yz}^+ = \frac{1}{2}\vec{\nabla} \wedge \vec{V}^+ \times \vec{x} = \frac{1}{2}\left(\frac{\partial w^+}{\partial y^+} - \frac{\partial v^+}{\partial z^+}\right) \quad (4)$$

Some of the typical structures presented in Fig. 1 can be identified. The most energetic leeward structure, Γ_A, is visible in all excerpts and, in the case of the squareback vehicle, the roof structure Γ_C is also evident. The Γ_C structure has actually been partly detected in the fastback vehicle as well, as indicates the non-zero vorticity region near the roof. Indeed, we have verified with steady crosswind tests and wool tufts that the roof vortex τ_C is aspirated towards the rear window, because of the low pressure induced by the latter. Hence, this structure is, for the most part, hidden in the masked PIV region. As far as the main structure Γ_A is concerned, it is stronger in the case of squareback vehicle, as the higher vorticity value suggests. The temporal evolutions of Γ_A

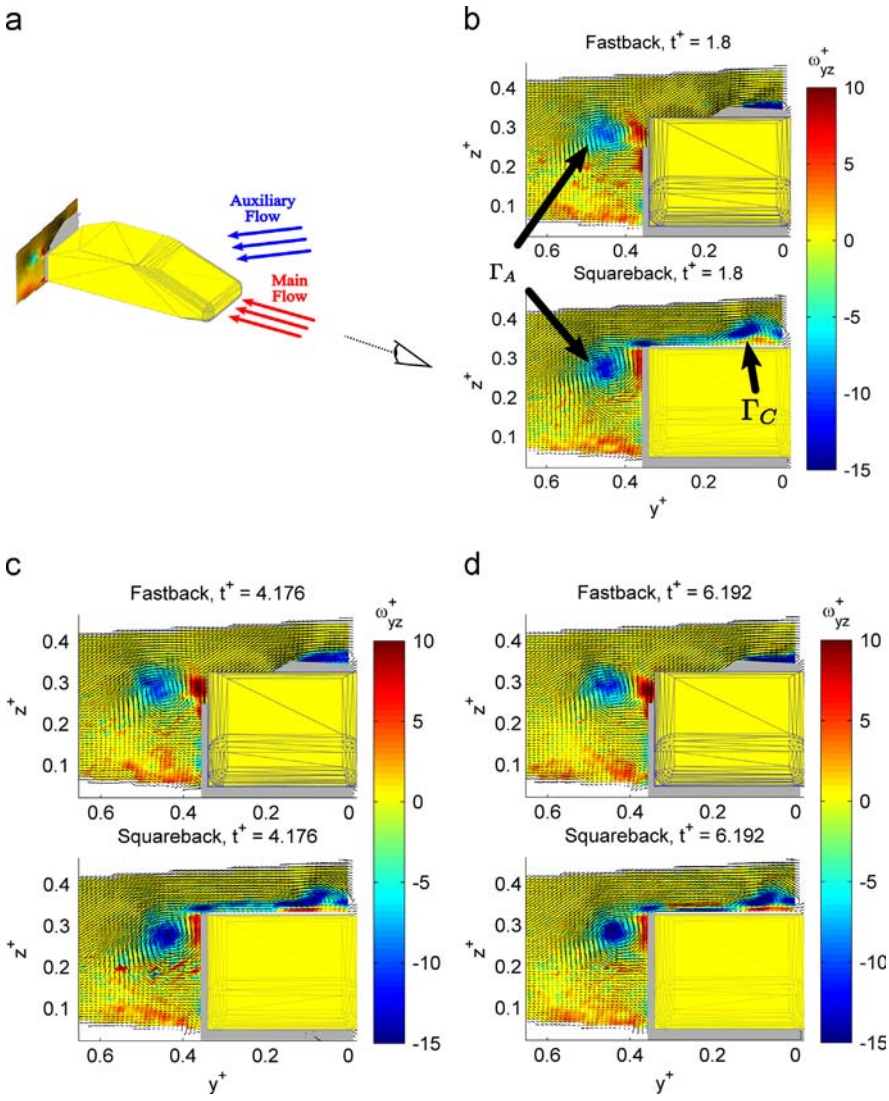

Fig. 13. Unsteady crosswind, stereoscopic PIV measurements of the non-dimensional vorticity flow field: perspective view, (a), $t^+ = 1.8$ (b), $t^+ = 4.176$, (c). $t^+ = 6.192$, (d).

center coordinates, calculated from the Q-criterion (Hunt et al., 1988), are reported in Fig. 14. The standard deviations of the center coordinates (represented by the error bars) indicate run to run variations. The average position of this vortex presents a transitory period before converging progressively towards established properties. It seems that the different rear geometry has little influence on Γ_A position as long as $t^+ < 3$, that is when the yaw moment and side force unsteady variations are evident. Afterward, it appears that the Γ_A center is statistically more distant to the leeward flank for the fastback geometry. This means that the fastback rear window does not affect the force unsteady variations, but rather their established values.

An interpretation for the Γ_A vortex center being farther to the vehicle is proposed in the schematic drawing in Fig. 15. When the fastback vehicle is yawed, the rooftop vortex Γ_C tends to merge with the longitudinal vortex developing from the rear window, vortex $\Gamma_{1,WW}$. Their union results in the formation of a greater and more energetic structure that that covers the total rear window region whereas the leeward vortex Γ_A tends to go away from the flank. In the case of the squareback vehicle the $\Gamma_{1,WW}$ vortex does not exist: the rooftop structure is then confined towards the windward part of the vehicle and cannot interact with Γ_C, which remains near the leeward flank.

The vertical structure τ_A being the most important structure in a plane of constant x^+ coordinate, its circulation may be correlated to the local side local efforts (Kutta–Joukowski theorem). In Fig. 16, the temporal evolution of the τ_A structure circulation is compared to the one of the global lateral efforts. The circulation is defined as:

$$\gamma^+ = \oint_{\partial C} \vec{V}^+ \times d\vec{l} = \iint_D \vec{\nabla} \wedge \vec{V}^+ \times \vec{n}\, dS = 2\iint_D \omega_{yz}^+ dS \quad \text{with} \quad \vec{n} = \begin{pmatrix} 1 \\ 0 \\ 0 \end{pmatrix} \tag{5}$$

where $d\vec{l}$ is the displacement vector, tangent to the circle ∂C and $\vec{n}$ the vector normal to the disk D bounded by $\partial C\left(\vec{n} = \vec{x}^+\right)$. It can be noticed the γ^+ temporal evolution is similar to those of the global aerodynamic forces. In particular, the circulation reaches maximum at the same time than the side force and the second yaw moment peak, at $t^+ = 3.096$. The correlation coefficient, r, has been then calculated:

$$r = \frac{Cov(C_E; \gamma^+)}{\sigma_{C_E} \sigma_{\gamma^+}} \tag{6}$$

where "Cov" is the covariance operator, σ the considered quantity standard deviation and C_E the effort coefficient (either C_{Fy} or C_{Mz}).

The results are presented in Table 1. It is shown that the Γ_A circulation transient evolution has a good correlation with the one of the yaw moment, becoming stronger when the side force is considered. This indicates that, when a vehicle is subjected to a sudden yaw angle change, the contribution of unsteady evolution of the Γ_A on lateral forces is important. In particular, its effect is predominant at vehicle's rear, as shown in Fig. 12c.

5. Conclusions

In this paper, a moving lateral flow double wind tunnel was used to generate an unsteady crosswind over a simplified car body. The goal was to simulate a sudden yaw angle change, similar to those observed when a side wind gust is crossed. The unsteady lateral aerodynamic efforts were measured and the flow evolution was studied by means of TR-PIV and synchronised stereoscopic PIV. Our objectives were the measurement of the lateral aerodynamic coefficients transitories, and perform a study on the transient flow organisation during the crosswind exposition.

Analyses were applied on two Windsor models, differing from the rear geometry. As far as side force and yaw moment are concerned, overshoots occurred after the gust arrival, as already observed in literature. Indeed, yaw moment coefficients exceed the corresponding steady values up to 16% and 10% respectively for the squareback and the fastback geometries. For the side force coefficients, these overshoots reach 7%. The lateral aerodynamic coefficients establish after the vehicle has travelled 7 times its own length, independently of the vehicle geometry.

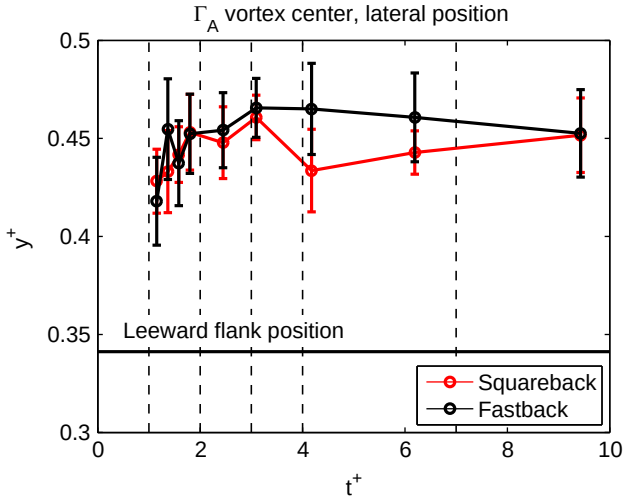

Fig. 14. Unsteady crosswind, lateral position of the Γ_A structure center, derived from stereoscopic PIV measurements. The error bars represent the position standard deviation.

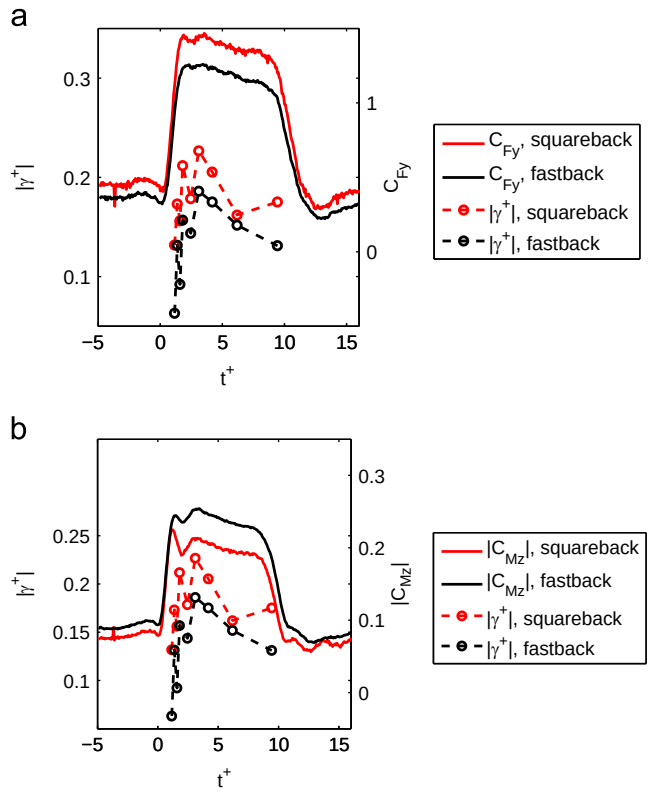

Fig. 16. Unsteady crosswind, comparison between the evolution of the non-dimensional circulation γ^+ of the Γ_A vortex and the aerodynamic efforts. Side force (a) and yaw moment (b).

Table 1
Correlation coefficients between circulation $\gamma+$ and lateral efforts for, both experimental and numerical results.

	Squareback (%)	Fastback (%)
C_{Fy}	$r=80.6$	$r=88.3$
C_{Mz}	$r=55.1$	$r=75.8$

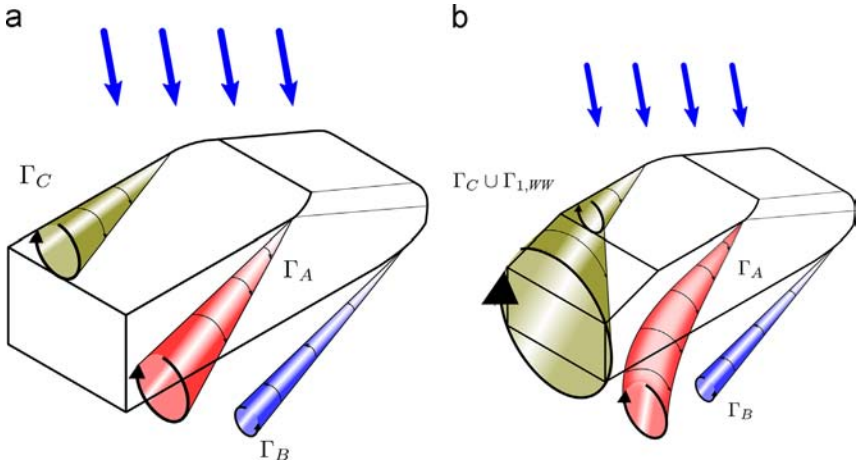

Fig. 15. Vortex pattern when the flow field is established: fastback vehicle (a), squareback vehicle, (b).

Our investigations on the flow field indicate that transient variations are mainly found in the region located at the rear of the vehicle leeward side. In particular, the local velocity temporal fluctuations measured in a horizontal mid-plane appear consistent with the lateral coefficients temporal evolutions. Also, the strength of the most energetic structure in the leeward side, Γ_A, has proved to be an important unsteadiness source. As a matter of fact, a good correlation has been found between the temporal evolution of this vortex circulation and the ones of the side force and yaw moment.

Moreover, the rear vehicle geometry has little impact on the flow and forces transient response but on the established values.

Further researches, replacing the synchronised stereoscopic PIV system with a complete stereoscopic time resolved PIV system should complete the unsteady data base and allow going further into the analysis of the correlation between the side force and the Γ_A circulation.

References

Ahmed, S., Ramm, R., Faltin, G., 1984. Some Salient Features of the Time-Averaged Ground Vehicle Wake. SAE Technical Paper No. 840300.

Baker, C.J., 1986. A simplified analysis of various types of wind induced road vehicle accidents. J. Wind Eng. Ind. Aerodyn. 22, 69–85.

Baker, C.J., 1991a. Ground vehicles in high cross winds Part I: Steady aerodynamic forces. J. Fluids Struct. 5, 69–90b.

Baker, C.J., 1991b. Ground vehicles in high cross winds Part II: Unsteady aerodynamic forces. J. Fluids Struct. 5, 91–111a.

Baker, C.J., 2010. The simulation of unsteady aerodynamic cross wind forces on trains. J. Wind Eng. Ind. Aerodyn. 98, 88–99.

Baker, C.J., Humphreys, N.D., 1996. Assessment of the adequacy of various wind tunnel techniques to obtain aerodynamic data for ground vehicles in cross winds. J. Wind Eng. Ind. Aerodyn. 60, 49–68.

Bearman, P., Mullarkey, S., 1994. Aerodynamic forces on road vehicles due to steady side winds and gusts. In: RAeS Conference on Vehicle Aerodynamics, Loughborough, UK.

Beauvais, F., 1967. Transient Nature of Wind Gust Effects on an Automobile. SAE Technical Paper No. 670608.

Cairns, R. S., 1994. Lateral Aerodynamic Characteristics of Motor Vehicles in Transient Crosswinds. Ph.D. Thesis. Cranfield University, UK.

Chadwick, A., 1999. Crosswind Aerodynamics of Sports Utility Vehicles. Ph.D. Thesis. Cranfield University, UK.

Chiu, T., Squire, L., 1992. An experimental study of the flow over a train in a crosswind at large yaw angles up to 90°. J. Wind Eng. Ind. Aerodyn. 45, 47–74.

Chometon, F., Strzelecki, A., Ferrand, V., Dechipre, H., Dufour, P.C., Gohlke, M., Herbert, V., 2005. Experimental Study of Unsteady Wakes Behind an Oscillating Car Model. SAE Technical Paper No. 2005-01-0604.

Clarke, J., Filippone, A., 2007. Unsteady computational analysis of vehicle passing. J. Fluids Eng. 129, 359–367.

Cooper, R., 1984. Atmospheric turbulence with respect to moving ground vehicles. J. Wind Eng. Ind. Aerodyn. 17, 215–238.

Corin, R., He, L., Dominy, R., 2008. A CFD investigation into the transient aerodynamic forces on overtaking road vehicle models. J. Wind Eng. Ind. Aerodyn. 96, 1390–1411.

Dominy, R., 1991. A technique for the investigation of transient aerodynamic forces on road vehicles in cross winds. ARCHIVE: Pro. Inst. Mech. Eng., Part D: J. Autom. Eng. 1989–1996 203–210 (205), 245–250.

Dominy, R., Ryan, A., 1999. An Improved Wind Tunnel Configuration for the Investigation of Aerodynamic Crosswind Gust Response. SAE Technical Paper No. 1999-01-0808.

Emmelmann, H., 1998. Driving stability in side winds. In: Hucho, W. (Ed.), Aerodynamics of Road Vehicles, SAE International, pp. 214–235 (ISBN 0–7680-0029-7)

Favre, T., Efraimsson, G., 2011. An assessment of detached-eddy simulations of unsteady crosswind aerodynamics of road vehicles. Flow Turbul. Combust. 87, 133–163.

Ferrand, V., Grochal, B., Forces and flow structures on a simplified car model exposed to a transient crosswind. In: Proceedings of the ASME 2012 Fluids Engineering Summer Meeting, Rio Grande, Puerto Rico, July 8–12, 2012.

Garry, K.P., Cooper, K.R., 1986. Comparison of quasi-static and dynamic wind tunnel measurements on simplified tractor-trailer models. J. Wind Eng. Ind. Aerodyn. 22, 185–194.

Gilliéron, P., Kourta, A., 2011. Aérodynamique automobile pour l'environnement, le design et la sécurité, (Ed.), Cépaduès, Toulouse, ISBN:9782854289695.

Hémon, P., Noger, C., 2004. Transient growth of energy and aeroelastic stability of ground vehicles. Comptes Rendus Mécanique 332, 175–180.

Howell, J., 1993. Shape features which influence crosswind sensitivity. In: Proceedings of the Institution of Mechanical Engineers, IMechE 1993-9, Vehicle Ride and Handling, 43–52.

Hunt, J.C.R., Wray, A.A., Moin, P., 1988. Eddies, Stream, and Convergence Zones in Turbulent Flows. Center for Turbulence Research Report CTR-S88, 193–208.

Khier, W., Breuer, M., Durst, F., 2000. Flow structure around trains under side wind conditions: a numerical study. Comput. Fluids 29, 179–195.

Kobayashi, N., Yamada, M., 1988. Stability of a One Box Type Vehicle in a Cross-Wind-An Analysis of Transient Aerodynamic Forces and Moments. SAE Technical Paper No. 881878.

Krajnovic, S., Ringqvist, P., Nakade, K., Basara, B., 2012. Large eddy simulation of the flow around a simplified train moving through a crosswind flow. J. Wind Eng. Ind. Aerodyn. 110, 86–99.

Mair, W., Stewart, A., 1985. The flow past yawed slender bodies, with and without ground effects. J. Wind Eng. Ind. Aerodyn. 18, 301–328.

Nakashima, T., Tsubokura, M., Vázquez, M., Owen, H., Doi, Y., 2012. Coupled analysis of unsteady aerodynamics and vehicle motion of a road vehicle in windy conditions. Comput. Fluids, In press, corrected proof, http://dx.doi.org/10.1016/j.compfluid.2012.09.028.

Ryan, A., 2000. The Simulation of Transient Cross-wind Gusts and their Aerodynamic Influence on Passenger Cars. Ph.D. Thesis. University of Durham, UK.

Ryan, A., Dominy, R., 2000. Wake Surveys Behind a Passenger Car Subjected to a Transient Cross-wind Gust. SAE Technical Paper No. 2000-01-0874.

Stewart, M., 1977. Transient aerodynamic forces on simple road vehicle shapes in simulated cross-wind gusts. Motor Ind. Res. Assoc.

Tomasini, G., Cheli, F., 2013. Admittance function to evaluate aerodynamic loads on vehicles: experimental data and numerical model. J. Wind Eng. Ind. Aerodyn. 38, 92–106.

Tsubokura, M., Nakashima, T., Kitayama, M., Ikawa, Y., Doh, D.H., Kobayashi, T., 2010. Large eddy simulation on the unsteady aerodynamic response of a road vehicle in transient crosswinds. Int. J. Heat Fluid Flow 31, 1075–1086.

Volpe, R., Da Silva, A., Ferrand, V., Le Moyne, L., 2013. Experimental and numerical validation of a wind gust facility. J. Fluid Eng., 135.